

## Formation of unsaturated carbon chains through carbon chemisorption on solid CO

MASASHI TSUGE,<sup>1</sup> GERMÁN MOLPECERES,<sup>2</sup> RYOTA ICHIMURA,<sup>3,4</sup> HIDEKO NOMURA,<sup>3</sup> KENJI FURUYA,<sup>5</sup> AND NAOKI WATANABE<sup>1</sup>

<sup>1</sup>*Institute of Low Temperature Science, Hokkaido University, Sapporo 060-0819, Kita-19 Nishi-8, Kita-ku, Sapporo 060-0819, Japan*

<sup>2</sup>*Departamento de Astrofísica Molecular, Instituto de Física Fundamental (IFF-CSIC), C/ Serrano 121, 123, 113B E-28006 Madrid, Spain*

<sup>3</sup>*Division of Science, National Astronomical Observatory of Japan, 2-21-1 Osawa, Mitaka, 181-8588, Japan*

<sup>4</sup>*Department of Astronomical Science, The Graduate University for Advanced Studies, SOKENDAI, 2-21-1 Osawa, Mitaka, 181-8588, Japan*

<sup>5</sup>*RIKEN Pioneering Research Institute, 2-1 Hirosawa, Wako, 351-0198, Japan*

(Received September 23, 2025; Revised September 23, 2025; Accepted September 23, 2025)

Submitted to ApJ

### ABSTRACT

The interaction of carbon atoms with solid carbon monoxide (CO) is a fundamental process in astrochemistry, influencing the formation of complex organic molecules in interstellar environments. This study investigates the adsorption and reaction mechanisms of carbon atoms on solid CO under cryogenic conditions, employing a combination of experimental techniques, including the combination of photostimulated desorption and resonance-enhanced multiphoton ionization (PSD-REMPI) and infrared spectroscopy, alongside quantum chemical calculations. The results reveal the formation of oxygenated carbon chains, such as CCO, C<sub>3</sub>O<sub>2</sub>, and C<sub>5</sub>O<sub>2</sub>, as well as CO<sub>2</sub>. The findings highlight the role of chemisorption and subsequent reactions in driving molecular complexity on solid CO, with implications for the chemical evolution of interstellar ices and the potential formation of prebiotic molecules.

### 1. INTRODUCTION

Carbon monoxide (CO) holds a unique position among interstellar molecules. It is not only the second most abundant molecule in the interstellar medium (ISM) after molecular hydrogen but also serves as a key precursor for the formation of interstellar complex organic molecules (COMs) (E. Herbst & E. F. Van Dishoeck 2009). A prominent example is the synthesis of interstellar methanol (CH<sub>3</sub>OH), one of the most iconic organic molecules in space, which occurs via the hydrogenation of CO (CO + 4H → CH<sub>3</sub>OH) on ice-covered submicron-sized dust grains (N. Watanabe & A. Kouchi 2002; M. Tsuge & N. Watanabe 2023). These icy grains form under the extremely low temperatures of dark molecular clouds (approximately 10 K), with their chemical composition evolving over time to represent different ice epochs (A. C. Boogert et al. 2015). The morphology of these ices during these epochs remains uncertain. Some studies propose that interstellar ices are stratified in an onion-like structure (A. C. Boogert et al. 2015), where an apolar layer forms atop a polar one, primarily composed of water, due to the differing timescales for polar and apolar material formation. Other studies suggest that different ice phases coex-

ist without fully wetting the grain's surface area (A. Potapov et al. 2020; A. Kouchi et al. 2021a,b). Regardless of the ice morphology, CO is expected to be the second most abundant constituent of interstellar ices and partially exist as CO solid. Therefore, interaction of adsorbates with CO solid plays a critical role in various chemical processes at the ice-gas interface.

To simulate energetic processes on interstellar icy grains, the irradiation of solid CO with electrons, protons, ultraviolet (UV) photons, heavy ions, and X-rays, has been extensively investigated in laboratory settings (C. S. Jamieson et al. 2006; M. Förstel et al. 2016; A. Trottier & R. L. Brooks 2004; P. A. Gerakines et al. 1996; N.-E. Sie et al. 2022; E. Seperuelo Duarte et al. 2010; A. Ciaravella et al. 2016). Under high-energy irradiation, the observed chemical processes are primarily attributed to the dissociation of CO molecules: CO(X<sup>1</sup>Σ<sup>+</sup>) → C(<sup>3</sup>P/<sup>1</sup>D) + O(<sup>3</sup>P/<sup>1</sup>D). The resulting C(<sup>3</sup>P/<sup>1</sup>D) atoms (hereafter designated as <sup>3</sup>C and <sup>1</sup>C) readily react with neighboring CO molecules to form <sup>3</sup>CCO, the simplest carbon chain intermediate. This species can subsequently undergo further reactions, initiating an oligomerization process. Specifically, C<sub>n</sub>O species (where n ≥ 2) can react with either atomic carbon or CO to yield C<sub>n+1</sub>O or C<sub>n+1</sub>O<sub>2</sub>, respectively (C. S. Jamieson et al. 2006). In the case of UV irradiation with photon energies below 11 eV (the dissociation energy of CO), photodesorption is the dom-

inant process (N.-E. Sie et al. 2022). However, the formation of CO<sub>2</sub> has also been observed. This phenomenon has been attributed to reactions involving excited CO (CO\*), such as CO\* + CO  $\longrightarrow$  CO<sub>2</sub> + C or, more generally, CO\* + C<sub>n</sub>O  $\longrightarrow$  CO<sub>2</sub> + C<sub>n</sub> (J. A. DeVine et al. 2022).

A completely different paradigm for chemistry on ices, particularly solid H<sub>2</sub>O and CO, involves the continuous accretion of atoms and small molecular species onto ice grains, a process characteristic of dark interstellar clouds. In these environments, adsorption of material occurs more frequently than photodissociation on icy due to the low permeability of photons in dark clouds. Some of the most common adsorbates landing on interstellar CO include atoms such as H, C, O, and N. The traditional view of surface astrochemistry assumes that these adsorbates remain physisorbed on the ice surface, where they can diffuse and react with other species following the Langmuir–Hinshelwood mechanism (W. Tielens 1982). In this context, hydrogenation reactions are considered the most significant pathway for increasing chemical complexity on icy grains, owing to the high mobility of hydrogen atoms (T. Hama et al. 2012; Y. Kimura et al. 2018) and their ability to quantum tunnel through kinetic barriers. Recent refinements of the diffusive mechanism include non-thermal scenarios, where newly formed molecules can transiently diffuse (M. Jin & R. T. Garrod 2020). The behavior of fundamental species other than H atom, such as C, O, and N atoms, has not been studied in as much detail. Among these, the C atom is particularly important because its reactions with other species can induce skeletal evolution of molecules, such as C–C bond formation (M. Tsuge et al. 2023). Especially intriguing is the duality exhibited by C atoms, as demonstrated in their behavior on water ice. In this case, C atoms can either remain physisorbed, facilitating molecular evolution, or chemisorb through an Eley–Rideal mechanism, depending on the adsorption binding site. This duality opens entirely different chemical pathways for the formation of complex molecules (M. Tsuge & N. Watanabe 2023; M. Tsuge et al. 2023; S. Ferrero et al. 2024; G. Molpeceres et al. 2021).

The reaction of C atoms with CO in a low-temperature solid has been recently studied both experimentally (G. Fedoseev et al. 2022), and theoretically (S. Ferrero et al. 2023a). G. Fedoseev et al. (2022) performed experiments where H/C/CO/H<sub>2</sub>O were simultaneously deposited at cryogenic temperatures. Under these conditions, they observed the formation of ketene (H<sub>2</sub>CCO), leading them to conclude that the CCO molecule formed by the reaction  $^3\text{C} + ^1\text{CO} \longrightarrow ^3\text{CCO}$  was subsequently hydrogenated to produce H<sub>2</sub>CCO. Although this pathway is very plausible under their experimental conditions, direct evidence for the formation of  $^3\text{CCO}$  was not presented. S. A. Krasnokutski et al. (2022) performed co-deposition of C/CO/NH<sub>3</sub> and observed infrared features at-

tributable to molecules with a C=C=O moiety. However, no definitive assignments were given in their paper. The formation of CCO and related products was later investigated computationally (S. Ferrero et al. 2023a). In this work, we employ our novel experimental setup to detect surface adatoms at cryogenic temperatures (M. Tsuge et al. 2023, 2024), posing the question of whether co-deposition experiments fully reflect the chemistry occurring under the conditions of cold dark clouds or even protoplanetary discs, which are characterized by a slow accretion of molecular material into solid bodies. In co-deposition experiments, rapid deposition of reactants facilitates immediate reactions. Recently, M. Tsuge et al. (2024) demonstrated that methane (CH<sub>4</sub>) production yield on the surface of amorphous solid water (ASW) is significantly different depending on the deposition method; co-deposition of C and H atoms yielded almost 100% conversion of C atoms into methane, whereas sequential deposition (C atom deposition followed by H atom deposition) resulted in less than 10% conversion. If the same paradigm-changing conclusions found for water ice are repeated in solid CO, it would change our view on the formation of unsaturated carbon chains, which is traditionally attributed to gas-phase chemistry (N. Sakai & S. Yamamoto 2013). To shed light on this conundrum, we undertook the task of simulating the adsorption of carbon atoms on solid CO. To succeed in this task, we applied the combination of photostimulated desorption and resonance-enhanced multiphoton ionization methods (PSD-REMPI) for the *in situ* detection of C atoms on solid CO, in combination with tailored quantum chemical calculations of reactivity. The reaction products in the sequential deposition (C atom deposition on solid CO) and co-deposition experiments were studied by infrared (IR) spectroscopy, including isotopic labeling. More details on Methodology are given in Section 2.

## 2. METHODS

### 2.1. Experimental Apparatus

All experiments were performed using the apparatus named RASCAL (Reaction Apparatus for Surface Characteristic Analysis at Low-temperature) at the Institute of Low Temperature Science, Hokkaido University. The details of RASCAL have been provided in previous works (T. Hama et al. 2012; N. Watanabe et al. 2010). RASCAL consists of an ultrahigh vacuum main chamber (with a base pressure of  $\sim 10^{-8}$  Pa) and a differentially pumped one for the C-atom source chamber. The aluminum (Al) substrate was positioned at the center of the main chamber and can be cooled to 5.5 K using a closed-cycle He refrigerator (RDK-415E, Sumitomo Heavy Industries). Temperature of the substrate was controlled using a silicon-diode temperature sensor (DT-670, Lake Shore), ceramic heaters (MC1020, Sakaguchi E.

H VOC), and a temperature controller (Model 335, Lake Shore).

A commercial C-atom source (SUKO-A, MBE-Komponenten) was used to provide exclusively C[1] in its electronic ground state; hence, no C atom clusters such as C<sub>3</sub> are emitted from the source. The most significant contaminant from the source was CO, which is presumably in the electronic ground state with ro-vibrational excitations considering the energy levels and source temperature above 2000 K. The flux of the C atom was controlled by adjusting the temperature of the filament, which comprised a thin Ta tube filled with carbon powder. The flux was determined by co-depositing C atoms and excess O<sub>2</sub>, where one O<sub>3</sub> molecule, which can be quantified by IR spectroscopy, is produced from one C atom ( $C + O_2 \longrightarrow CO + O$ ;  $O + O_2 \longrightarrow O_3$ ); i.e., the C-atom flux was calculated by dividing the column density of O<sub>3</sub> by deposition time.

## 2.2. Preparation of amorphous solid CO

The amorphous solid CO samples were produced via background vapor deposition of CO molecules at a substrate temperature of 10 K. The deposition rate was approximately 1 monolayer (ML) min<sup>-1</sup>, corresponding to the flux of  $\sim 2 \times 10^{13}$  atoms cm<sup>-2</sup> s<sup>-1</sup>. This flux is slightly above the critical flux for the formation of amorphous CO at 10 K (A. Kouchi et al. 2021a). In the PSD-REMPI measurements, CO solid with 5 MLs thickness were initially prepared and after each measurement additional 2-3 MLs were deposited to refresh the surface condition; this procedure was repeated for five to six measurements and after that the sample was sublimated.

## 2.3. C-atom detection by PSD-REMPI

The PSD-REMPI method has been successfully applied to detect trace reactive species such as H atoms and OH radicals on the surface of dust grain analogues (K. Kuwahata et al. 2015; A. Miyazaki et al. 2020; N.-E. Sie et al. 2024). Carbon atoms on solid CO were desorbed by weak nanosecond laser pulse at 532 nm (10 Hz repetition rate) with the typical pulse energy of 80  $\mu$ J. The C atoms desorbed from the surface were then ionized by the REMPI laser that was focused approximately 1 mm above the Al substrate with the timing that achieves the maximum PSD-REMPI signals. At the focal point of the REMPI laser, C atoms were ionized using the (2+1)REMPI scheme via the  $2s^2 2p 3p(^3D_3) \leftarrow 2s^2 2p^2(^3P_2)$  transition (J. D. Fassett et al. 1985). Laser radiation in the wavelength range 286.8–286.9 nm with a pulse energy of approximately 1 mJ was provided from an Nd<sup>3+</sup>:YAG laser-pumped dye laser, with subsequent frequency doubling with a potassium dihydrogen phosphate crystal. The ionized C atom (C<sup>+</sup>) was then detected by a linear type time-of-flight mass spectrometer equipped with a micro-channel plate detector.

## 2.4. Infrared measurements

The IR spectra of the samples on the Al substrate were measured using reflection-absorption IR spectrometry with a Fourier-transform infrared spectrometer (Spectrum One, Perkin Elmer) equipped with a KBr beam splitter and an Hg–Cd–Te detector. Spectra in a region of 700–4000 cm<sup>-1</sup> were collected at a resolution of 4 cm<sup>-1</sup> after averaging 200 or 400 scans. The surface number density (column density) of species X, denoted as [X] in molecules cm<sup>-2</sup>, was estimated using the following equation:

$$[X] = \frac{\cos(\theta) \ln 10}{2B} \int_{\nu_1}^{\nu_2} A(\nu) d\nu \quad (1)$$

where  $\theta$ ,  $B$ , and  $A(\nu)$  represent the incident angle of the IR beam with respect to the Al substrate (83°), integrated absorption coefficient (in the unit of cm molecule<sup>-1</sup>), and absorbance at a given wavenumber, respectively. The  $B$  values for CO<sub>2</sub> ( $\nu_3$ ,  $B = 1.0 \times 10^{-16}$ ), CCO ( $\nu_1$ ,  $B = 2.3 \times 10^{-17}$ ), C<sub>3</sub>O<sub>2</sub> ( $\nu_3$ ,  $B = 4.9 \times 10^{-16}$ ), and C<sub>5</sub>O<sub>2</sub> ( $\nu_4$ ,  $B = 1.1 \times 10^{-17}$ ) were calculated at the B3LYP/cc-pVTZ level of theory. These calculated values agreed very well with those provided by C. S. Jamieson et al. (2006) based on their own B3LYP/6-311G\*\* calculations. Although experimental  $B$  values have been reported for solid CO<sub>2</sub> and C<sub>3</sub>O<sub>2</sub>, we used calculated value for consistency among all the species. value for CO<sub>2</sub> agreed well with the reported experimental value of  $1.8 \times 10^{-16}$  (P. A. Gerakines & R. L. Hudson 2015). On the other hand, the  $B$  value calculated for C<sub>3</sub>O<sub>2</sub> is several times greater than the experimental value of  $1.3 \times 10^{-16}$  (P. Gerakines & M. Moore 2001); this difference might originate from the fact that calculation was done for isolated molecule and experimental value is for the pure solid of C<sub>3</sub>O<sub>2</sub>. We thus indicate that the C<sub>3</sub>O<sub>2</sub> number density derived using calculated  $B$  value could be overestimated.

## 2.5. Quantum Chemical Calculations

To mimic the conditions of the sequential deposition experiments we studied the reaction of <sup>3</sup>C with solid CO under high dilution conditions. To achieve that, we used a cluster model mimicking the local environment of a CO, extracted from our previous work (G. Molpeceres et al. 2023a), containing 33 CO molecules. The level of theory throughout the calculations is also equivalent to that of that work (i.e. DLPNO-CCSD(T)/CBS//MN15(D3BJ)/6-31+G(d,p)) (C. Riplinger et al. 2016; Y. Guo et al. 2018; S. Zhong et al. 2008; F. Neese & E. F. Valeev 2011; H. S. Yu et al. 2016; S. Grimme et al. 2010, 2011; T. Clark et al. 1983), where CBS stands for complete basis set (extrapolation), that we achieved with a two-point formula and DLPNO-CCSD calculations using the cc-pVDZ and cc-pVTZ basis-sets (D. E. Woon & T. H. Dunning 1994). The initial cluster structure is optimized at the MN15(D3BJ)/6-31+G(d,p) on top of

which DLPNO-CCSD(T)/CBS single point calculations are performed. The reaction of C atoms with solid CO is simulated placing the atoms in random positions of the cluster and performing a force minimization. The chemisorption energy of the C atom is calculated as the difference between the energy of the cluster with the C atom and the energy of the cluster and carbon atoms separated. A similar procedure is later carried out, but now placing a  $C_2$  molecule close to a CCO chemisorbate, in order to investigate  $C_5O_2$  formation. The evolution of the chemisorbates reacting with a neighbor CO molecule is computed by performing potential energy scans along the reaction coordinate, and optimizing the local maxima found during the scan. Activation energies are then computed as the difference between the energy at the transition state and of the chemisorbate. All energies reported in this work include harmonic vibrational zero point energy corrections. The uncertainties in the energies correspond to the standard deviation of the energetic magnitudes in the three sampled binding sites. Geometry optimizations and frequency calculations were performed using the GAUSSIAN 16 program (M. J. Frisch et al. 2016). The DLPNO-CCSD(T) calculations were performed using the ORCA 6.0.0 (F. Neese 2012; F. Neese et al. 2020) program.

### 3. EXPERIMENTAL RESULTS

#### 3.1. Characterization of C atoms on solid CO

In panel (a) of Figure 1, we show the PSD-REMPI intensity of  $^{13}C$  atoms, which is proportional to the surface number density, as a function of C-atom deposition time. The increasing rate of signal intensity gradually decelerates towards saturation. This behavior is similar to that observed for C atoms on ASW (M. Tsuge et al. 2023) and indicates physical processes that reduce the number of detectable carbon atoms. This behavior on ASW was attributed to the conversion of C atoms from a physisorbed state to a chemisorbed one (M. Tsuge et al. 2023). By analogy, it is anticipated that the formation of the  $^{13}CCO$  molecule from C atoms physisorbed on solid CO might be the primary loss process, as predicted by theoretical studies (S. Ferrero et al. 2023a). The physisorbed states in our experiment cannot be clearly isolated contrary to our works on  $H_2O$  ice (M. Tsuge et al. 2023, 2024), because they transiently convert to chemisorbed ones, which is the unique state at the end of the experiment, and therefore the most interesting one from the astrochemical perspective. Among other possible loss processes, thermal desorption should be negligible at 10 K, considering that much lighter species such as hydrogen atoms and  $H_2$  can also remain on the surface of solid CO at this temperature.

After the deposition of C atoms was completed, a continuous decrease in C-atom intensity was clearly observed (Figure 1, panel b). Decay profiles were recorded for various deposition times 100, 200, and 400 s, corresponding to the C-

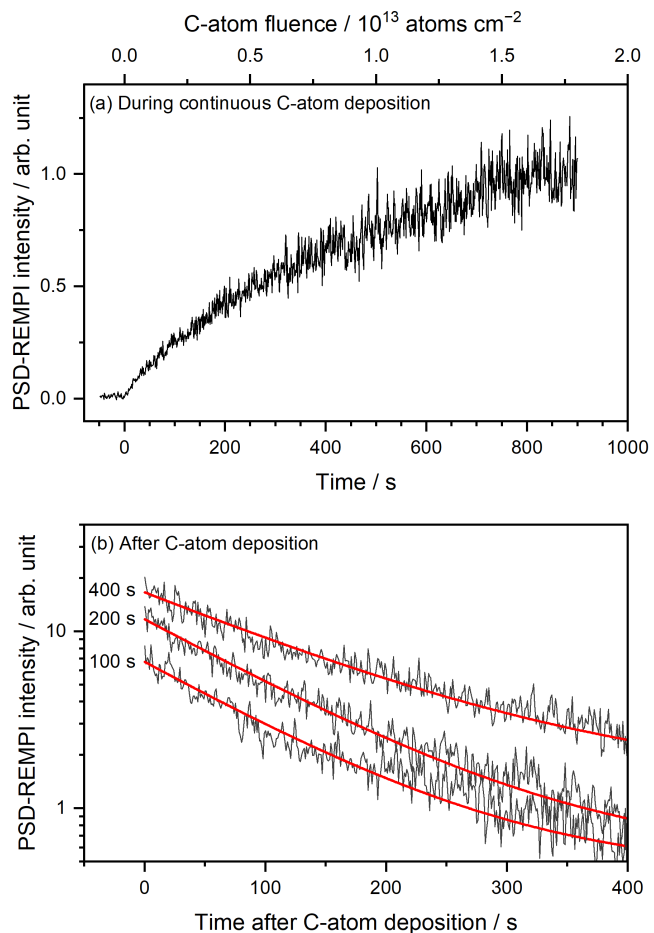


**Figure 1.** In situ C-atom detection by PSD-REMPI. (a) The PSD-REMPI intensity of C-atoms during continuous C-atom deposition on solid CO at 10 K with the C-atom flux of  $2 \times 10^{10}$  atoms  $cm^{-2} s^{-1}$ . (b) The decay of PSD-REMPI intensity after terminating C-atom deposition; after 100 s deposition (bottom), 200 s (middle), and 400 s (top) deposition, corresponding to the C-atom fluences of  $2 \times 10^{12}$ ,  $4 \times 10^{12}$ ,  $8 \times 10^{12}$  atoms  $cm^{-2}$ , respectively. Black lines are experimental data and red lines represent the fitting result according to Equation 2.

atom fluences of  $2 \times 10^{12}$ ,  $4 \times 10^{12}$ , and  $8 \times 10^{12}$  atoms  $cm^{-2}$ . The decay profiles were well described by a single exponential function, indicating that the decay process follows first-order reaction kinetics. The exponential function is expressed as:

$$[C]_t = [C]_0 [(1 - b) \exp(-kt) + b] \quad (2)$$

where  $[C]_t$  and  $[C]_0$  represent the surface number density of C atoms at time  $t$  and  $t = 0$ , respectively,  $k$  is the decay rate, and  $b$  is an asymptotic value indicating the fraction of C atoms that remain on the surface at infinite time. Due to the non-zero  $b$  values ( $b = 0.05-0.1$ ), the fitted curve is not a straight line even in the logarithmic scale plot. The  $k$  values for deposition times of 100, 200, and 400 s were determined to be



$(1.0 \pm 0.2) \times 10^{-2}$ ,  $(7.7 \pm 1.2) \times 10^{-3}$ , and  $(6.3 \pm 1.2) \times 10^{-3}$   $\text{s}^{-1}$ , respectively. These decay rates correspond to decay time constants ( $1/k$ ) of  $100 \pm 20$ ,  $130 \pm 20$ , and  $160 \pm 30$  s, respectively. The errors represent statistical uncertainties across seven measurements.

We also analyzed the decay curves assuming the C-atom loss by diffusive recombination reaction ( $2\text{C} \longrightarrow \text{C}_2$ ). In this case,  $[\text{C}]_t$  can be expressed as:

$$\frac{[\text{C}]_0}{[\text{C}]_t} = 2k_{\text{diff}} [\text{C}]_0 t + 1 \quad (3)$$

where  $k_{\text{diff}}$  is the surface diffusion rate constant of C atoms on solid CO. For C-atom deposition durations of 100 and 400 s, the values of  $2 \cdot k_{\text{diff}} \cdot [\text{C}]_0$  were determined to be  $0.012 \pm 0.006$  and  $0.010 \pm 0.002$   $\text{s}^{-1}$ , respectively. According to the experimental data presented in Figure 1a, the ratio of  $[\text{C}]_0$  values after 100 and 400 s depositions,  $[\text{C}]_0(400 \text{ s})/[\text{C}]_0(100 \text{ s})$ , is approximately 2.9. Under the assumption that the C-atom binding energy distribution is coverage-independent, the  $k_{\text{diff}}$  value should also be coverage-independent. Consequently, the  $2 \cdot k_{\text{diff}} \cdot [\text{C}]_0$  value for the 400 s deposition should be about three times as large as that for the 100 s deposition if the C-atom decay is due to diffusive recombination. However, these values are consistent within statistical errors, indicating that diffusive recombination is not responsible for the observed C-atom decay. Therefore, any source of detectable C-atom loss must arise from processes other than C–C recombination. We propose that the only process responsible for the C-atom decay is the formation of  $^3\text{CCO}$ , where the rate-limiting step is likely either the short-distance diffusion of C atoms to locate reactive CO or the  $^3\text{C} + \text{CO} \longrightarrow ^3\text{CCO}$  reaction itself.

In order to get further insights into the decay process, its temperature dependence was studied. The decay profiles were measured at 5.5, 10, 15, and 20 K with 200 s deposition time. The C-atom decay rates at these temperatures were determined to be  $(6.9 \pm 1.0) \times 10^{-3}$ ,  $(7.7 \pm 1.2) \times 10^{-3}$ ,  $(7.1 \pm 0.5) \times 10^{-3}$ , and  $(7.1 \pm 1.0) \times 10^{-3}$   $\text{s}^{-1}$ , respectively. Hence, no temperature dependence was observed for the C-atom decay in the temperature range of 5.5–20 K, meaning that the C-atom decay proceeds by non-thermal mechanisms, such as quantum mechanical tunneling or barrierless reactions. A temperature-independent decay was also observed for C atoms on ASW (M. Tsuge et al. 2023). In that case, the conversion from physisorbed to chemisorbed states by quantum mechanical tunneling was suggested as the most plausible process responsible for the decay, while the involvement of short-distance C-atom diffusion was excluded based on the experimentally determined activation energy for surface diffusion ( $E_{\text{sd}} = 1020$  K). Neither the activation energy for surface diffusion ( $E_{\text{sd}}$ ) nor for desorption ( $E_{\text{des}}$ ) has been reported for C atoms on solid CO. Moreover, as described

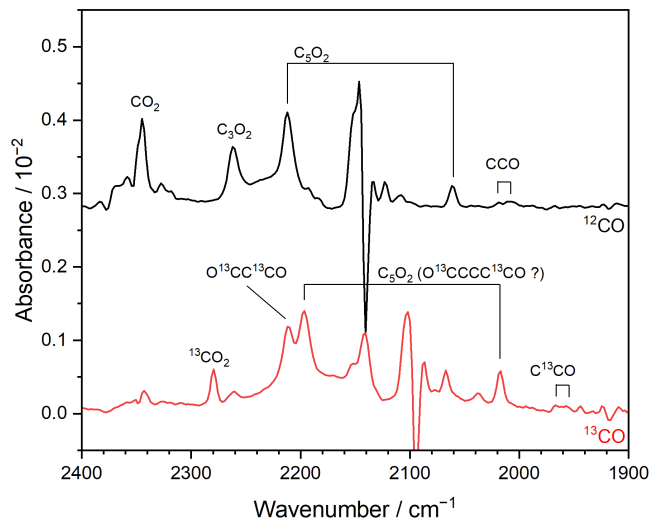


**Figure 2.** IR difference spectra measured after depositing C atoms on solid  $^{12}\text{CO}$  (upper trace) and on solid  $^{13}\text{CO}$  (bottom trace) at 10 K. The thickness of solid CO was about 10 MLs and the C-atom fluence was about  $7 \times 10^{13}$  atoms  $\text{cm}^{-2}$ . Spectral assignments for  $\text{CO}_2$ ,  $\text{C}_3\text{O}_2$ ,  $\text{C}_5\text{O}_2$ , and  $\text{CCO}$  are presented. Isotopic composition of  $\text{C}_5\text{O}_2$  in  $^{13}\text{CO}$  experiment is uncertain (see text).

in Section 4, quantum chemical calculations suggest that the  $^3\text{C} + \text{CO}$  reaction producing  $^3\text{CCO}$  is barrierless. Therefore, we exclude quantum tunneling of C atoms as the primary reaction driver. Interestingly, quantum tunneling might still play an indirect role in the decay of the C atom signal in our experiment. As demonstrated by A. Choudhury et al. (2022), CO molecules undergo orientational isomerization (i.e., flipping of the CO dipole) at low temperatures via quantum tunneling on laboratory timescales. These timescales align remarkably well with our experimental observations, suggesting that the reactivity of C atoms may depend on the orientation of CO molecules. Specifically, C–CO orientations are immediately reactive (as shown in Section 4), while C–OC orientations are unreactive and require CO flipping via the aforementioned tunneling mechanism to enable reactions.

In addition to IR spectroscopy (shown in Section 3.2), we attempted to detect  $^3\text{CCO}$  on solid CO using the PSD-REMPI method, but without success. We employed PSD laser wavelengths of 532 nm or 355 nm, along with a REMPI laser wavelength of 450–453 nm (P. J. Tjossem & T. A. Cool 1985). The non-detection of  $^3\text{CCO}$  could be attributed to either (i)  $^3\text{CCO}$  not being desorbed by the 532 nm or 355 nm PSD laser, or (ii) the lifetime of  $^3\text{CCO}$  being too short, resulting in its surface number density falling below the detection limit due to rapid conversion, e.g., into  $\text{C}_3\text{O}_2$  (see Sections 3.2 and 4). It is worth noting, however, that the reference for REMPI detection was obtained from gas-phase studies (P. J. Tjossem & T. A. Cool 1985).

### 3.2. Sequential deposition experiments

Since the primary reaction product of the C + CO reaction,  ${}^3\text{CCO}$ , could not be identified using the PSD-REMPI method, we conducted measurements of IR spectra. These measurements involved both the sequential deposition of C atoms on solid CO (this section) and the co-deposition of C atoms and CO (Section 3.3). The sequential deposition closely resembles the PSD-REMPI experiments and is more representative of astrophysical conditions.

The upper trace of Figure 2 shows the IR difference spectrum after 60 minutes of C-atom deposition on solids of  ${}^{12}\text{CO}$  and  ${}^{13}\text{CO}$  at 10 K, with C-atoms fluence of approximately  $7 \times 10^{13} \text{ atoms cm}^{-2}$ . Here,  ${}^{12}\text{CO}$  and  ${}^{13}\text{CO}$  refer to the normal CO sample (natural  ${}^{13}\text{C}/{}^{12}\text{C}$  ratio) and the  ${}^{13}\text{C}$ -enriched sample (99.2 atom%), respectively. In the spectrum obtained for solid  ${}^{12}\text{CO}$  (upper trace), intense peaks were observed at 2062, 2212, 2262, and 2345  $\text{cm}^{-1}$ , along with a weak feature near 2008  $\text{cm}^{-1}$ . The peak at 2345  $\text{cm}^{-1}$  is clearly attributed to  $\text{CO}_2$ . Based on literature values (P. Gerakines & M. Moore 2001; C. S. Jamieson et al. 2006; A. Trottier & R. L. Brooks 2004; A. C. Boogert et al. 2015), the peaks at 2062 and 2212  $\text{cm}^{-1}$  were assigned to  $\text{C}_5\text{O}_2$ , the peak at 2262  $\text{cm}^{-1}$  to  $\text{C}_3\text{O}_2$ , and the weak feature at 2008  $\text{cm}^{-1}$  to CCO. The spectrum measured for solid  ${}^{13}\text{CO}$  (Figure 2, lower trace) also supports these assignments. The intensities of the peaks corresponding to products, except for CCO, increased with deposition time, whereas the intensity of the CCO peak reached its maximum after 20–30 minutes, corresponding to a C-atom fluence of  $2\text{--}4 \times 10^{13} \text{ atoms cm}^{-2}$ , and remained nearly constant thereafter. Using calculated absorption coefficients (see Section 2.4), the following column densities were estimated for a C-atom fluence of approximately  $7 \times 10^{13} \text{ atoms cm}^{-2}$ : CCO,  $5.3 \times 10^{12} \text{ cm}^{-2}$ ;  $\text{C}_3\text{O}_2$ ,  $6.5 \times 10^{12} \text{ cm}^{-2}$ ;  $\text{C}_5\text{O}_2$ ,  $2.0 \times 10^{12} \text{ cm}^{-2}$ ; and  $\text{CO}_2$ ,  $1.6 \times 10^{13} \text{ cm}^{-2}$ . These column density estimates are uncertain because absorption coefficients calculated for gas-phase species were used, except for  $\text{CO}_2$  (P. A. Gerakines & R. L. Hudson 2015). For  $\text{C}_3\text{O}_2$ , an experimental absorption coefficient has been reported ( $1.3 \times 10^{-16} \text{ cm molecule}^{-1}$ ), and using this value, the column density of  $\text{C}_3\text{O}_2$  is calculated to be  $2.4 \times 10^{13} \text{ cm}^{-2}$ . As described below, the  $\text{CO}_2$  product does not incorporate deposited C atoms (i.e., the carbon in  $\text{CO}_2$  originates from CO molecules). Therefore, the major species produced by consuming C atoms in the sequential deposition experiments is  $\text{C}_3\text{O}_2$ . For comparison, we also performed C-atom deposition on crystalline CO ( $\alpha\text{-CO}$ ) solid at 10 K, but no significant differences were observed between amorphous and crystalline CO solids.

### 3.3. Co-deposition experiments

Co-deposition experiments have been often conducted because reactant molecules are well mixed and have more

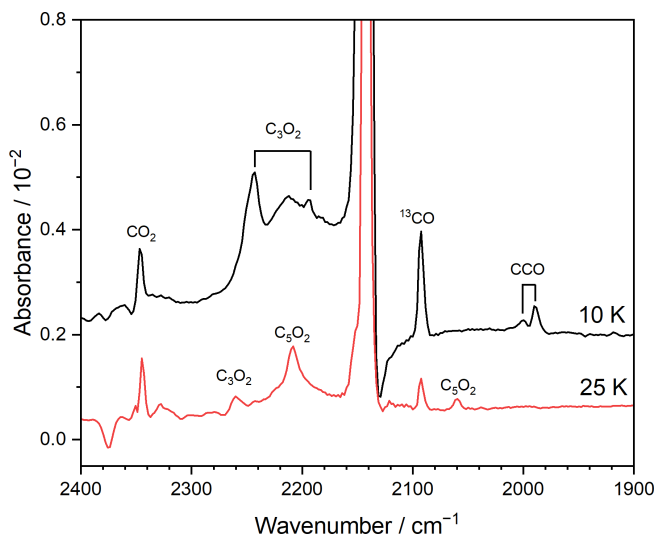


**Figure 3.** IR spectra measured in the C/CO co-deposition experiments. Deposition at 10 K and deposition at 25 K (lower trace). The C/CO ratio was approximately 1/1000 and the C-atom fluence was about  $5 \times 10^{13} \text{ atoms cm}^{-2}$ . Spectral assignments for  $\text{CO}_2$ ,  $\text{C}_3\text{O}_2$ ,  $\text{C}_5\text{O}_2$ , and CCO are presented.

chances to encounter during accumulation on the surface, leading to higher reaction yields. We performed co-deposition of C atoms and CO for comparison, particularly with the study of G. Fedoseev et al. (2022), which identified the formation of ketene ( $\text{H}_2\text{CCO}$ ) in H/C/CO/ $\text{H}_2\text{O}$  mixtures.

The upper trace of Figure 3 shows the IR spectrum measured after co-deposition of C atoms and CO (1/1000 dilution) at 10 K for 40 minutes, where the C-atom fluence was approximately  $5 \times 10^{13} \text{ atoms cm}^{-2}$ . In the spectrum, a broad feature spanning from 2160–2300  $\text{cm}^{-1}$  is the phonon wing of solid CO. In this spectral region, two peaks were identified at 2195 and 2243  $\text{cm}^{-1}$  and are assigned to  $\text{C}_3\text{O}_2$ . The absence of any features near 2062  $\text{cm}^{-1}$ , which was observed in the sequential deposition experiment (see Figure 2), indicates that  $\text{C}_5\text{O}_2$  was absent in this sample. The IR features attributable to CCO were observed at 1990 and 2000  $\text{cm}^{-1}$ . In addition,  $\text{CO}_2$  was observed at 2347  $\text{cm}^{-1}$  similarly to the sequential deposition experiments. Column densities of these products were estimated for a C-atom fluence of about  $5 \times 10^{13} \text{ atoms cm}^{-2}$ : CCO,  $7.3 \times 10^{13} \text{ cm}^{-2}$ ;  $\text{C}_3\text{O}_2$ ,  $9.2 \times 10^{12} \text{ cm}^{-2}$ ;  $\text{CO}_2$ ,  $1.4 \times 10^{13} \text{ cm}^{-2}$ . The CCO yield exceeds the C-atom fluence most probably because the CCO column density was overestimated. Nonetheless, CCO seems to be the major product in the C/CO co-deposition conditions. It should be noted that the CCO formation is significantly enhanced when C and CO were co-deposited probably because of rapid dissipation of reaction energy as high as 53.7  $\text{kcal mol}^{-1}$  (Section 4). G. Fedoseev et al. (2022) reported that co-deposition of H/C/CO/ $\text{H}_2\text{O}$  yielded ketene ( $\text{H}_2\text{CCO}$ ) and  $\text{C}_3\text{O}_2$  was absent in their spectra, indicating

that hydrogenation of CCO occurred readily so that  $\text{CCO} + \text{CO} \longrightarrow \text{C}_3\text{O}_2$  is hindered. Consequently, we suspect that ketene formation is enhanced only under laboratory conditions, where the CCO product is readily thermalized and H atoms are abundant. Under molecular cloud conditions, typical H atom accretion rate to each grain is one H atom per day. Thus, the timescale for the H atom reaction is significantly longer than that of  $\text{CCO} + \text{CO} \longrightarrow \text{C}_3\text{O}_2$ , whose timescale is shorter than that of the energy dissipation process. Finally, we note that experimental conditions are quite different between this work and [G. Fedoseev et al. \(2022\)](#); C-atom flux was about 25 times larger than ours, the C/CO ratio of their work was approximately 1/2, and  $\text{H}_2\text{O}$  was the dominant component.

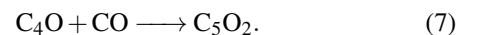
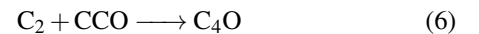
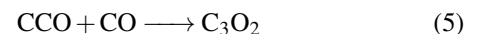
The spectrum obtained after the deposition of a C/CO = 1/1000 mixture at 25 K for 40 minutes is shown as the lower trace of Figure 3. The ratio of  $^{13}\text{CO}$  intensity between 10 and 25 K indicates that the adsorption coefficient of CO molecules is several times smaller at 25 K. The peaks at 2060 and 2208  $\text{cm}^{-1}$  are assigned to  $\text{C}_5\text{O}_2$ , while the peak at 2260  $\text{cm}^{-1}$  is attributed to  $\text{C}_3\text{O}_2$ . The difference in the peak position for  $\text{C}_3\text{O}_2$  between 10 K and 25 K is due to the differing crystallinity of the solid CO; it is amorphous at 10 K and crystalline at 25 K. The amounts of these products were proportional to the deposition time. Notably, CCO was absent in the 25 K sample. Since the formation of  $\text{C}_3\text{O}_2$  is most likely due to the reaction  $\text{CCO} + \text{CO} \longrightarrow \text{C}_3\text{O}_2$ , CCO should still form at 25 K but is rapidly consumed to produce  $\text{C}_3\text{O}_2$ . The formation mechanisms for  $\text{C}_5\text{O}_2$  remain unclear. Stoichiometrically, three C atoms and two CO molecules are required to produce  $\text{C}_5\text{O}_2$ . The absence of  $\text{C}_5\text{O}_2$  at 10 K and its presence at 25 K suggest that thermal processes play a role in  $\text{C}_5\text{O}_2$  production. Given the low C-atom flux in the experiment ( $2 \times 10^{10} \text{ atoms cm}^{-2} \text{ s}^{-1}$ ), the simultaneous involvement of three C atoms at a single reaction site is unlikely without some enhanced surface mobility (e.g., at 10 K). The most plausible explanation involves the formation of  $\text{C}_2$  molecules through the  $\text{C} + \text{C} \longrightarrow \text{C}_2$  non-thermal reaction in the experimental setup, followed by a barrierless addition to a neighboring CCO molecule; i.e.,  $\text{C}_2 + \text{CCO} \longrightarrow \text{C}_4\text{O}$ ,  $\text{C}_4\text{O} + \text{CO} \longrightarrow \text{C}_5\text{O}_2$ . This mechanism explains the enhanced abundance of  $\text{C}_5\text{O}_2$  at 25 K. This is the mechanism simulated in our quantum chemical calculations (see Section 4), where it is shown to be effective. An alternative reaction mechanism could involve  $\text{C}_n\text{O}$  ( $n = 2, 3$ ) species reacting with CO to produce  $\text{C}_n$  and  $\text{CO}_2$ :  $\text{C}_n\text{O} + \text{CO} \longrightarrow \text{C}_n + \text{CO}_2$ . Although this reaction is expected to be endothermic, the heat of reaction at the formation of  $\text{C}_n\text{O}$  species, i.e.,  $\text{C}_{n-1} + \text{CO} \longrightarrow \text{C}_n\text{O}$ , could induce this reaction. Interestingly, however, this mechanism suggests that a single C atom can trigger the formation of several  $\text{CO}_2$  molecules,

aligning with the relatively high yield of  $\text{CO}_2$  observed in both sequential and co-deposition experiments.

#### 4. DISCUSSION

The combined results from the three sets of experiments (Section 3) reveal a rather complex chemical reaction network for C atoms adsorbed on solid CO that requires explanation. In previous studies, [G. Fedoseev et al. \(2022\)](#) primarily reported the formation of  $\text{H}_2\text{CCO}$  in a co-deposition experiment involving C/CO/H, a finding further supported by theoretical calculations from [S. Ferrero et al. \(2023a\)](#). However, in the more diluted environment explored in this work, the lack of accessible H atoms prevents the formation of  $\text{H}_2\text{CCO}$ . As a result, in the absence of such rapid hydrogen-driven chemistry, we observe the non-energetic formation of unsaturated carbon chains, a process previously suggested only in ices exposed to energetic irradiation ([C. S. Jamieson et al. 2006](#); [M. Förstel et al. 2016](#); [A. Trottier & R. L. Brooks 2004](#); [N.-E. Sie et al. 2022](#); [E. Seperuelo Duarte et al. 2010](#); [A. Ciaravella et al. 2016](#)), but shown to extend to cold, non-energetic chemistry. As demonstrated in Sections 3.2 and 3.3, our experiments reveal the synthesis of a diverse array of carbon chains, including CCO,  $\text{C}_3\text{O}_2$ , and  $\text{C}_5\text{O}_2$ , as well as  $\text{CO}_2$ . From an astrochemical perspective, identifying the atomistic processes responsible for the formation of these species is crucial for understanding their contribution to the total carbon chain budget in solid CO.

To help in identifying the specific atomistic processes that contribute to the formation of every possible carbon chain we have conducted a quantum chemical investigation trying to replicate the experiments in the laboratory. In the first place, we attempted to simulate the formation of the CCO,  $\text{C}_3\text{O}_2$ , and  $\text{C}_5\text{O}_2$  carbon chains. For that, the following reactions are considered:



From these reactions, reaction 4 is the one directly transferable to the ISM, whereas reaction 6 requires a localized concentration of C atoms, which is less likely to occur in real astronomical ices (see the discussions below).

For reaction 4, we initiated simulations by randomly placing a carbon atom in its electronic ground state (i.e.,  $\text{C}(^3\text{P})$ ) within a pre-optimized ice model consisting of 33 CO molecules (see Section 2.5). This procedure was repeated for three distinct binding sites to gather statistical insights. In all cases, the simulations consistently showed the direct formation of CCO in its triplet state, aligning with prior theoretical predictions ([S. Ferrero et al. 2023a](#)). The force minimization

process revealed that the reaction proceeds via a C–CO interaction. Experimentally, however, C–OC adsorption is also possible. This geometry does not directly lead to reaction and requires CO dipole flipping (A. Choudhury et al. 2022), which can explain the observed time-dependent behavior in our experiments.

The starting geometries for the subsequent calculations are shown in Figure 4, upper panel. The average adsorption energy,  $\Delta U_R$ , was determined to be  $-53.7 \pm 0.6$  kcal mol $^{-1}$ , which is approximately 4 kcal mol $^{-1}$  higher than the reported gas-phase value (A. Papakondylis & A. Mavridis 2019). This excess energy must correspond to the binding energy between  $^3\text{CCO}$  and CO. The chemisorption energy can be utilized in various ways, including transient diffusion on the CO ice, desorption, surface reconstruction or reaction with a neighboring CO molecule. While the first three processes are challenging to detect experimentally, the latter is straightforward to identify, as it corresponds to reaction 5. Using the three binding geometries shown in Figure 4, we examined reaction 5, as depicted in the bottom panel of the figure for Site I. Notably, the electronic ground state of  $\text{C}_3\text{O}_2$  is a singlet, whereas CCO is a triplet. To simulate reaction 5, we first considered the formation of  $^3\text{C}_3\text{O}_2$ , followed by an intersystem crossing that aligns with laboratory timescales, leading to  $^1\text{C}_3\text{O}_2$ . The activation energy,  $\Delta U_a$ , for reaction 5 in the triplet channel was found to be  $7.5 \pm 0.7$  kcal mol $^{-1}$ , representing, on average, 13.9% of the total available chemisorption energy. The  $\Delta U_R$  for the  $^3\text{CCO} + \text{CO} \longrightarrow ^3\text{C}_3\text{O}_2$  reaction was  $-7.9 \pm 0.7$  kcal mol $^{-1}$ . Although limited information is available on chemical energy relaxation in solid CO, recent studies on vibrational energy relaxation (B. C. Ferrari et al. 2024) suggest longer timescales than those observed in water ice (G. Molpeceres et al. 2023b; S. Ferrero et al. 2023b). This finding supports the argument for the rapid, non-thermal formation of  $^3\text{C}_3\text{O}_2$  through reaction 5 in sequential deposition experiments. Moreover, it also explains why a small fraction of CCO can be detected in experiments at 10 K, indicating a subset of binding sites with rapid energy dissipation. In co-deposition experiments, as shown in this work and by G. Fedoseev et al. (2022), CCO is present because this dissipation occurs more quickly, especially in the presence of water molecules. An important aspect concerns the competition between  $\text{C}_3\text{O}_2$  formation and the desorption of  $^3\text{CCO}$  after its generation, given that the estimated adsorption energy is only about 4 kcal mol $^{-1}$  (roughly 7.4% of the overall reaction energy), see above. While chemical desorption (or diffusion) cannot be ruled out, its quantitative assessment lies beyond the scope of both our experiments and calculations. Nevertheless, recent studies on energy dissipation, albeit on  $\text{H}_2\text{O}$  ice (G. Molpeceres et al. 2023b), demonstrate that the conversion of chemical energy from intramolecular modes into weak translational motion is highly

inefficient, typically remaining below 7%. In this context, the C=O stretching of  $^3\text{CCO}$ , which corresponds to the reaction coordinate of  $^3\text{CCO} + \text{CO} \longrightarrow ^3\text{C}_3\text{O}_2$ , is far more likely to channel the excess energy towards reaction rather than desorption. Finally, we did not explicitly simulate the triplet–singlet decay of  $\text{C}_3\text{O}_2$ , but it is a plausible outcome within laboratory (and astronomical) timescales, considering the experimental evidence and the significant exothermicity of the process, calculated to be  $-75.8 \pm 0.9$  kcal mol $^{-1}$ . A summary of the mechanism is shown in Figure 5.

The formation of  $\text{C}_5\text{O}_2$  cannot be easily explained with a single  $^3\text{C}$  adsorption, because Reaction 5 terminates the formation of the carbon chain. Likewise, successive addition of  $^3\text{C}$  on a carbon chain is unlikely. Another, possibly more likely, option involves the reaction of  $\text{C}_2$  formed during the deposition with CCO and subsequent reaction with a neighboring CO molecule. The mechanism for the formation of  $\text{C}_2$  might be due to direct association of two C atoms via a hot-atom mechanism. Regardless of the  $\text{C}_2$  formation mechanism, once formed it can react with CCO to yield  $\text{C}_4\text{O}$  via reaction 6. Calculations for this reaction involve a strongly multireference electronic structure, in which the  $\text{C}_2$  molecule has two closely spaced electronic states,  $^1\Sigma^+$  and  $^3\Pi_u$  (as exemplified in the review by A. J. C. Varandas & C. M. R. Rocha (2018)), therefore, our combined DFT and coupled cluster calculations should be viewed with caution, and only serve to prove a barrierless association between  $\text{C}_2$  and CCO. The calculations were performed placing a  $\text{C}_2$  molecule in the vicinity of a CCO radical ensuring a real electronic minimum in the triplet state through a wavefunction stability analysis, because the ground state of the  $\text{C}_4\text{O}$  molecule is a  $^3\Sigma^-$  state (H. Kannari et al. 1994; J. C. Rienstra-Kiracofe et al. 2000; C. S. Jamieson et al. 2006), and leaving the system evolve with a force minimization. In all cases, it was found that  $\text{C}_2$  evolves without barriers to  $\text{C}_4\text{O}$ . The depth of the  $\text{C}_4\text{O}$  well is  $-143.7 \pm 0.8$  kcal mol $^{-1}$ . Therefore, when  $\text{C}_2$  is close to CCO a spontaneous formation of  $^3\text{C}_4\text{O}$  takes place with an immense release of chemical energy. Once formed, the vast amount of reaction energy liberated in the association can be used to react with another neighboring CO molecule forming  $\text{C}_5\text{O}_2$  (Reaction 7, and equivalent to the scheme shown in Figure 4 bottom panel) with only a 5.5% of the association energy required for the reaction. Finally, the  $\Delta U_a$  in the triplet channel is  $7.9 \pm 0.4$  kcal mol $^{-1}$  ( $\Delta U_R = -13.1 \pm 1.1$  kcal mol $^{-1}$ ) and the triplet–singlet gap is  $-58.8 \pm 0.66$  kcal mol $^{-1}$ . Therefore, with this mechanism we explain the presence of  $\text{C}_5\text{O}_2$  in our reaction mixture and only  $\text{CO}_2$  remains to be explained. Regrettably, we could not explain the formation of  $\text{CO}_2$  in our simulations simply considering ground state chemistry, as we have done for all reactions in this section. It is well known that  $\text{CO}_2$  is readily formed by CO in an excited state in heavily processed ices (C. S. Jamieson



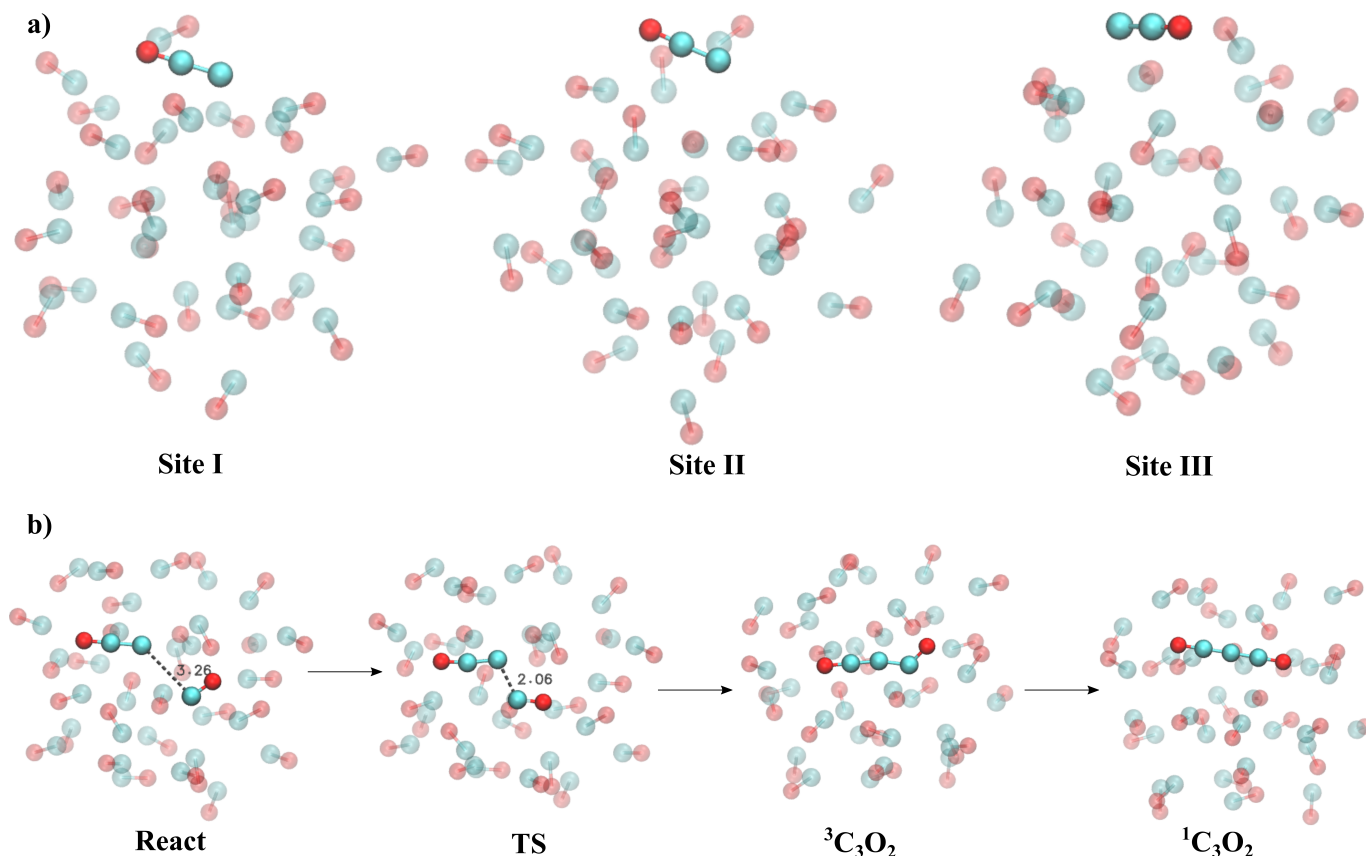


**Figure 4.** (a) Adsorption geometries of  $^3\text{C}$  on CO ice reflecting chemisorption and formation of the  $^3\text{CCO}$  complex on different binding sites at the DLPNO-CCSD(T)/CBS//MN15(D3BJ)/6-31+G(d,p) level. The individual values for the chemisorption energies are  $54.0 \text{ kcal mol}^{-1}$  for Site I,  $54.0 \text{ kcal mol}^{-1}$  for Site II and  $53.0 \text{ kcal mol}^{-1}$  for Site III. (b) Scheme of the  $\text{CCO} + \text{CO} \rightarrow \text{C}_3\text{O}_2$  reaction at Site I after  $^3\text{C}$  chemisorption.

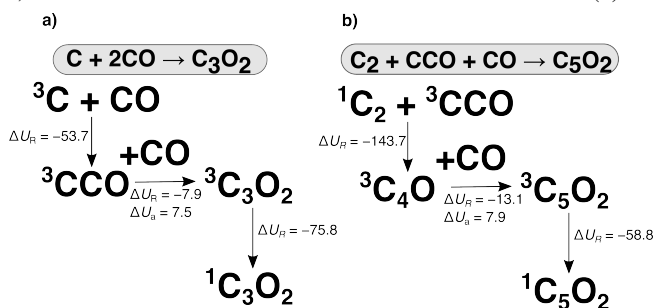


**Figure 5.** (a) Schematic view for the simulated reaction profile for the formation of  $\text{C}_3\text{O}_2$  (b) Suggested scheme for the formation of  $\text{C}_5\text{O}_2$  in our experiments.  $\Delta U_R$  and  $\Delta U_a$  represent the reaction energies and activation energies, if any, of the elementary steps showcased in the diagram. All energies are shown in  $\text{kcal mol}^{-1}$ .

et al. 2006; M. Förstel et al. 2016; A. Trottier & R. L. Brooks 2004; P. A. Gerakines et al. 1996; N.-E. Sie et al. 2022; E. Seperuelo Duarte et al. 2010; A. Ciaravella et al. 2016; J. A. DeVine et al. 2022). Our results suggest that the formation of  $\text{CO}_2$  in our experiments might be a consequence of the high energy released in the formation of the carbon chains, forming  $\text{C}_n$  and hence  $\text{CO}_2$  in the process. We consider the formation of  $\text{C}_n$  and  $\text{CO}_2$  hardly transferable to the

conditions of the ISM where the energy deposited by surface area is lower than in our experiments due to the lower accretion rate of C atoms. In summary, the formation of carbon chains observed in our experiments highlights the intricate chemical processes occurring on solid CO. However, the experimental conditions may not fully replicate the conditions prevalent in the ISM. Under ISM conditions, the formation of  $\text{C}_3\text{O}_2$  appears plausible based on our calculations. However, the synthesis of longer carbon chains, such as  $\text{C}_5\text{O}_2$ , or the production of  $\text{CO}_2$ , is less likely. From a physicochemical perspective, however, all the carbon chains identified in this study could theoretically form on nanosized icy grains. A schematic overview of the physicochemical and astrochemical pathways for carbon chain formation identified in this work is presented in Figure 6.

Based on our experiments and quantum chemical calculations, it becomes evident that astrochemical reaction network models should include the chemisorption of C atoms on CO ice as well as that on  $\text{H}_2\text{O}$  ice. However, the resulting chemical pathways are likely sensitive to the local distribution of CO on the ice surface—whether CO molecules are randomly distributed or aggregated. In astrochemical models based on the rate-equation approach, which is the most widely used

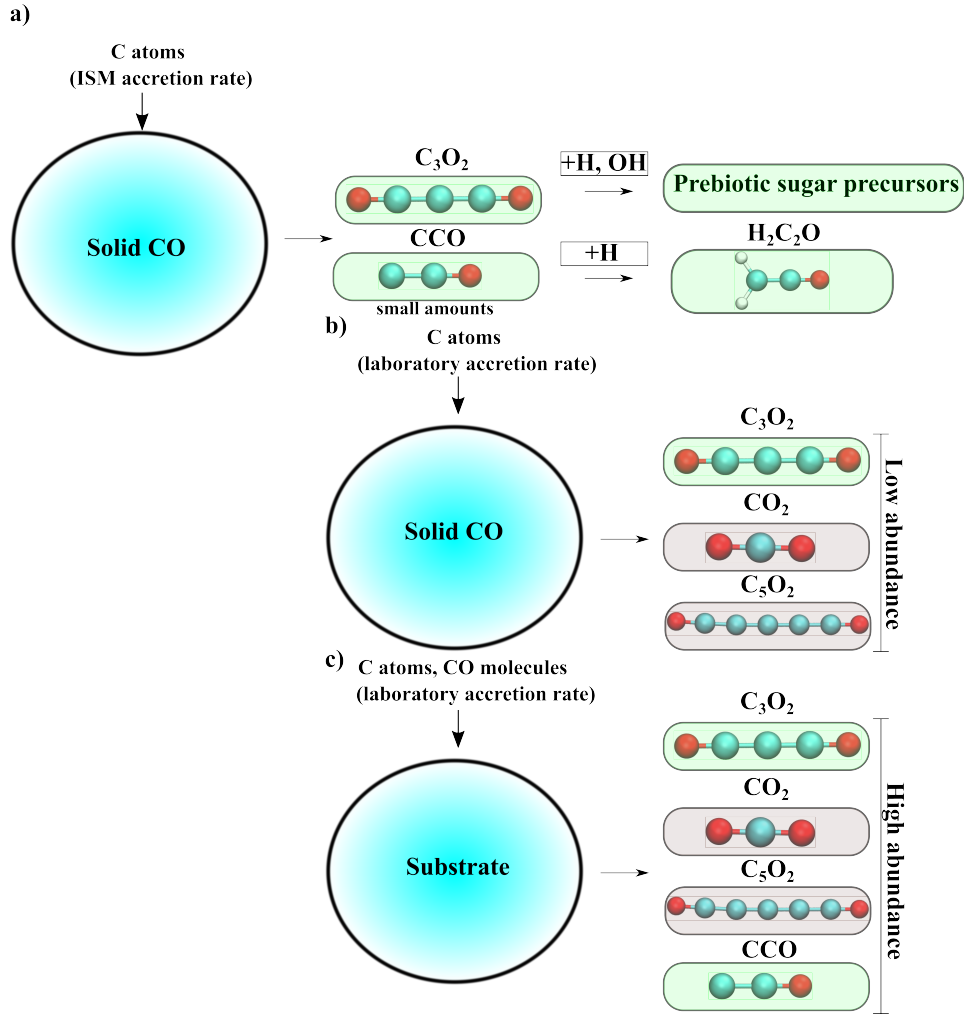


**Figure 6.** Schematic summary of our results. The figure illustrates the formation of oxygenated carbon chains,  $C_3O_2$ ,  $C_5O_2$ ,  $CCO$ , and  $CO_2$ . Panel (a) represents the ideal situation in the ISM with a low accretion rate of carbon atoms impinging the ice, panel (b) shows the exemplification of the sequential deposition experiments at 10 K and panel (c) the co-deposition experiments at 10-25 K. Pale green boxes represent molecules that are compatible with ISM dilution conditions whereas gray boxes represent molecules that are less likely to occur in the ISM.

method in the astrochemistry community, adsorbed species on surfaces are implicitly assumed to be randomly and homogeneously distributed, which favors isolated encounters with CO and thus the formation of  $H_2CCO$ , depending on the surface coverage of CO. The surface coverage of CO would depend on the physical environment and time, ranging from approximately  $< 10\%$  to  $\sim 70\%$  (V. Taquet et al. 2014; G. Molpeceres et al. 2024). On the other hand, if CO molecules are aggregated, as suggested by A. Kouchi et al. (2021a), the C-atom chemisorption on solid CO would lead to  $C_3O_2$ , as demonstrated by this work. To assess such effects, the use of the microscopic kinetic Monte Carlo (kMC) approach, which can explicitly account for the spatial arrangement of adsorbed species on surfaces (H. M. Cuppen et al. 2013; R. T. Garrod 2013), would be more appropriate than the rate-equation approach, especially in the low to medium coverage of CO.

To conclude, the  $C_3O_2$  molecule formed through this reaction chain in the ISM could serve as a precursor for further reactions under the unique conditions of interstellar ices. To our knowledge,  $C_3O_2$  has not been firmly identified in the ISM. However, R. J. Cartwright et al. (2024) discussed their possible detection by JWST/NIRSpec. According to their interpretation, the features observed at 4.41 and 4.47  $\mu m$  might be due to either  $C_3O_2$  (and higher order carbon chain oxides) or CN-bearing compounds known to exist in the irradiated ice containing carbon oxides and ammonia (G. Strazzulla et al. 2007).

Certainly, the conditions of our experiments and associated calculations are highly controlled, effectively restricting the chemical network under study to reactions involving carbon atoms, CO molecules, and their immediate products. In the interstellar medium, however, a far richer variety of reactive species is present, dramatically expand-

ing the chemical complexity that can emerge following the readily formation of CCO or  $C_3O_2$ . Of particular interest, as suggested by previous studies for the hydrogenation of  $C_2O$  (G. Fedoseev et al. 2022; S. Ferrero et al. 2023a), is the hydrogenation of  $C_3O_2$  facilitated by quantum tunneling. This process could lead to the formation of molecules such as  $H_2C_3O_2$ ,  $H_4C_3O_2$ ,  $H_6C_3O_2$ , or  $H_8C_3O_2$  (Figure 6). Beyond hydrogenation, reactions with other abundant radicals, particularly at the apolar-polar ice interface (A. C. Boogert et al. 2015), such as OH,  $NH_2$ , or  $CH_3$ , could yield even more complex molecules. These processes may significantly enhance the abundance of prebiotic molecules in interstellar ices. For instance, glycerol ( $C_3H_8O_3$ ), glyceraldehyde ( $HOCH_2CH(OH)CHO$ ), and glyceric acid ( $HOCH_2CH(OH)COOH$ ), which are important prebiotic molecules identified in laboratory ice experiments (R. I. Kaiser et al. 2015; G. Fedoseev et al. 2017; J. Wang et al. 2024), could be synthesized more efficiently due to the increased availability of  $C_3O_2$ .

## 5. CONCLUSION

In this work, combining experimental and theoretical approaches, we have demonstrated for the first time the plausibility of forming complex carbon chains through the non-energetic reaction of atomic carbon with ice, complementing other experiments indicating that energetic input was needed. A key aspect of our findings and discussions is that not all experimental evidence is directly transferable to the chemistry of the ISM, where dilution conditions are far more extreme than in any laboratory experiment. After a careful analysis grounded in quantum chemical calculations, we conclude that the formation of  $C_3O_2$  is the most likely reaction to occur

in the ISM, while the formation of  $C_5O_2$  and  $CO_2$  is likely an artifact of our experimental setup. We cannot rule out the stabilization of a small fraction of CCO at low temperatures in the ISM. The facile synthesis of  $C_3O_2$  in our experiments suggests that this molecule could serve as a precursor for the formation of more complex prebiotic sugars in real astrophysical environments. We emphasize the importance of fundamental physical chemistry in proposing, understanding, and interpreting our experiments, along with the integration of experiments and theory to provide a comprehensive understanding of the molecular Universe.

## ACKNOWLEDGMENTS

This work was partially supported by JSPS KAKENHI (grant Nos. JP25K07364, JP25KJ133, JP24K00686, JP23H03982, JP22H00159, and JP17H06087). G.M. acknowledges the support of the grant RYC2022-035442-I funded by MICIU/AEI/10.13039/501100011033 and ESF+. G.M. also received support from project 20245AT016 (Proyectos Intramurales CSIC). We acknowledge the computational resources provided by the DRAGO computer cluster managed by SGA-CSIC, and the Galician Supercomputing Center (CESGA). The supercomputer FinisTerra III and its permanent data storage system have been funded by the Spanish Ministry of Science and Innovation, the Galician Government and the European Regional Development Fund (ERDF).

*Facilities:* Cesga Supercomputer

*Software:* GAUSSIAN16 (M. J. Frisch et al. 2016), ORCA6.0.1 (F. Neese 2012; F. Neese et al. 2020)

## REFERENCES

- Boogert, A. C., Gerakines, P. A., & Whittet, D. C. 2015, *Ann. Rev. Astron. Astrophys.*, 53, 541, doi: [10.1146/annurev-astro-082214-122348](https://doi.org/10.1146/annurev-astro-082214-122348)
- Cartwright, R. J., Holler, B. J., Grundy, W. M., et al. 2024, *The Astrophysical Journal Letters*, 970, L29, doi: [10.3847/2041-8213/ad566a](https://doi.org/10.3847/2041-8213/ad566a)
- Choudhury, A., DeVine, J. A., Sinha, S., et al. 2022, *Nature*, 612, 691, doi: [10.1038/s41586-022-05451-0](https://doi.org/10.1038/s41586-022-05451-0)
- Ciaravella, A., Chen, Y.-J., Cecchi-Pestellini, C., et al. 2016, *Astrophys. J.*, 819, 38, doi: [10.3847/0004-637X/819/1/38](https://doi.org/10.3847/0004-637X/819/1/38)
- Clark, T., Chandrasekhar, J., Spitznagel, G. W., & Schleyer, P. V. R. 1983, *Journal of Computational Chemistry*, 4, 294, doi: [10.1002/jcc.540040303](https://doi.org/10.1002/jcc.540040303)
- Cuppen, H. M., Karssemeijer, L. J., & Lamberts, T. 2013, *Chemical Reviews*, 113, 8840, doi: [10.1021/cr400234a](https://doi.org/10.1021/cr400234a)
- DeVine, J. A., Choudhury, A., Lau, J. A., Schwarzer, D., & Wodtke, A. M. 2022, *The Journal of Physical Chemistry A*, 126, 2270, doi: [10.1021/acs.jpca.2c01168](https://doi.org/10.1021/acs.jpca.2c01168)
- Fassett, J. D., Moore, L. J., Travis, J. C., & DeVoe, J. R. 1985, *Science*, 230, 262, doi: [10.1126/science.230.4723.262](https://doi.org/10.1126/science.230.4723.262)
- Fedoseev, G., Chuang, K.-J., Ioppolo, S., et al. 2017, *The Astrophysical Journal*, 842, 52, doi: [10.3847/1538-4357/aa74dc](https://doi.org/10.3847/1538-4357/aa74dc)
- Fedoseev, G., Qasim, D., Chuang, K.-J., et al. 2022, *Astrophys. J.*, 924, 110, doi: [10.3847/1538-4357/ac3834](https://doi.org/10.3847/1538-4357/ac3834)
- Ferrari, B. C., Van Hemert, M., Meyer, J., & Lamberts, T. 2024, *J. Phys. Chem. C*, 128, 21060, doi: [10.1021/acs.jpcc.4c05232](https://doi.org/10.1021/acs.jpcc.4c05232)
- Ferrero, S., Ceccarelli, C., Ugliengo, P., Sodupe, M., & Rimola, A. 2023a, *Astrophys. J.*, 951, 150, doi: [10.3847/1538-4357/acd192](https://doi.org/10.3847/1538-4357/acd192)
- Ferrero, S., Ceccarelli, C., Ugliengo, P., Sodupe, M., & Rimola, A. 2024, *The Astrophysical Journal*, 960, 22, doi: [10.3847/1538-4357/ad0547](https://doi.org/10.3847/1538-4357/ad0547)

- Ferrero, S., Pantaleone, S., Ceccarelli, C., et al. 2023b, *The Astrophysical Journal*, 944, 142, doi: [10.3847/1538-4357/acae8e](https://doi.org/10.3847/1538-4357/acae8e)
- Frisch, M. J., Trucks, G. W., Schlegel, H. B., et al. 2016, Gaussian 16 Revision C.01, Gaussian, Inc., Wallingford CT
- Förstel, M., Maksyutenko, P., Mebel, A. M., & Kaiser, R. I. 2016, *Astrophys. J. Lett.*, 818, L30, doi: [10.3847/2041-8205/818/2/L30](https://doi.org/10.3847/2041-8205/818/2/L30)
- Garrod, R. T. 2013, *The Astrophysical Journal*, 778, 158, doi: [10.1088/0004-637X/778/2/158](https://doi.org/10.1088/0004-637X/778/2/158)
- Gerakines, P., & Moore, M. 2001, *Icarus*, 154, 372, doi: [10.1006/icar.2001.6711](https://doi.org/10.1006/icar.2001.6711)
- Gerakines, P. A., & Hudson, R. L. 2015, *Astrophys. J.*, 808, L40, doi: [10.1088/2041-8205/808/2/L40](https://doi.org/10.1088/2041-8205/808/2/L40)
- Gerakines, P. A., Schutte, W. A., & Ehrenfreund, P. 1996, *Astron. Astrophys.*, 312, 289
- Grimme, S., Antony, J., Ehrlich, S., & Krieg, H. 2010, *Journal of Chemical Physics*, 132, 154104, doi: [10.1063/1.3382344](https://doi.org/10.1063/1.3382344)
- Grimme, S., Ehrlich, S., & Goerigk, L. 2011, *Journal of Computational Chemistry*, 32, 1456, doi: <https://doi.org/10.1002/jcc.21759>
- Guo, Y., Riplinger, C., Becker, U., et al. 2018, *The Journal of Chemical Physics*, 148, 011101, doi: [10.1063/1.5011798](https://doi.org/10.1063/1.5011798)
- Hama, T., Kuwahata, K., Watanabe, N., et al. 2012, *Astrophys. J.*, 757, 185, doi: [10.1088/0004-637X/757/2/185](https://doi.org/10.1088/0004-637X/757/2/185)
- Herbst, E., & Van Dishoeck, E. F. 2009, *Annual Review of Astronomy and Astrophysics*, 47, 427, doi: [10.1146/annurev-astro-082708-101654](https://doi.org/10.1146/annurev-astro-082708-101654)
- Jamieson, C. S., Mebel, A. M., & Kaiser, R. I. 2006, *Astrophys. J. Supp. Ser.*, 163, 184, doi: [10.1086/499245](https://doi.org/10.1086/499245)
- Jin, M., & Garrod, R. T. 2020, *The Astrophysical Journal Supplement Series*, 249, 26, doi: [10.3847/1538-4365/ab9ec8](https://doi.org/10.3847/1538-4365/ab9ec8)
- Kaiser, R. I., Maity, S., & Jones, B. M. 2015, *Angewandte Chemie*, 127, 197, doi: [10.1002/ange.201408729](https://doi.org/10.1002/ange.201408729)
- Kannari, H., Aoki, K., Hashimoto, K., & Ikuta, S. 1994, *Chemical Physics Letters*, 222, 313, doi: [10.1016/0009-2614\(94\)87066-7](https://doi.org/10.1016/0009-2614(94)87066-7)
- Kimura, Y., Tsuge, M., Pirronello, V., Kouchi, A., & Watanabe, N. 2018, *Astrophys. J.*, 858, L23, doi: [10.3847/2041-8213/aac102](https://doi.org/10.3847/2041-8213/aac102)
- Kouchi, A., Tsuge, M., Hama, T., et al. 2021a, *Mon. Not. R. Astron. Soc.*, 505, 1530, doi: [10.1093/mnras/stab1173](https://doi.org/10.1093/mnras/stab1173)
- Kouchi, A., Tsuge, M., Hama, T., et al. 2021b, *Astrophys. J.*, 918, 45, doi: [10.3847/1538-4357/ac0ae6](https://doi.org/10.3847/1538-4357/ac0ae6)
- Krasnokutski, S. A., Chuang, K.-J., Jäger, C., Ueberschaar, N., & Henning, T. 2022, *Nature Astronomy*, 6, 381, doi: [10.1038/s41550-021-01577-9](https://doi.org/10.1038/s41550-021-01577-9)
- Kuwahata, K., Hama, T., Kouchi, A., & Watanabe, N. 2015, *Phys. Rev. Lett.*, 115, doi: [10.1103/PhysRevLett.115.133201](https://doi.org/10.1103/PhysRevLett.115.133201)
- Miyazaki, A., Watanabe, N., Sameera, W. M. C., et al. 2020, *Phys. Rev. A*, 102, 052822, doi: [10.1103/PhysRevA.102.052822](https://doi.org/10.1103/PhysRevA.102.052822)
- Molpeceres, G., Enrique-Romero, J., & Aikawa, Y. 2023a, *Astronomy & Astrophysics*, 677, A39, doi: [10.1051/0004-6361/202347097](https://doi.org/10.1051/0004-6361/202347097)
- Molpeceres, G., Furuya, K., & Aikawa, Y. 2024, *Astronomy & Astrophysics*, 688, A150, doi: [10.1051/0004-6361/202449604](https://doi.org/10.1051/0004-6361/202449604)
- Molpeceres, G., Kästner, J., Fedoseev, G., et al. 2021, *Journal of Physical Chemistry Letters*, 12, 10854, doi: [10.1021/acs.jpcclett.1c02760](https://doi.org/10.1021/acs.jpcclett.1c02760)
- Molpeceres, G., Zaverkin, V., Furuya, K., Aikawa, Y., & Kästner, J. 2023b, *Astronomy & Astrophysics*, 673, A51, doi: [10.1051/0004-6361/202346073](https://doi.org/10.1051/0004-6361/202346073)
- Neese, F. 2012, *WIREs Computational Molecular Science*, 2, 73, doi: [10.1002/wcms.81](https://doi.org/10.1002/wcms.81)
- Neese, F., & Valeev, E. F. 2011, *Journal of Chemical Theory and Computation*, 7, 33, doi: [10.1021/ct100396y](https://doi.org/10.1021/ct100396y)
- Neese, F., Wennmohs, F., Becker, U., & Riplinger, C. 2020, *Journal of Chemical Physics*, 152, 224108, doi: [10.1063/5.0004608](https://doi.org/10.1063/5.0004608)
- Papakondylis, A., & Mavridis, A. 2019, *The Journal of Physical Chemistry A*, 123, 10290, doi: [10.1021/acs.jpca.9b09084](https://doi.org/10.1021/acs.jpca.9b09084)
- Potapov, A., Jäger, C., & Henning, T. 2020, *Physical Review Letters*, 124, 221103, doi: [10.1103/PhysRevLett.124.221103](https://doi.org/10.1103/PhysRevLett.124.221103)
- Rienstra-Kiracofe, J. C., Ellison, G. B., Hoffman, B. C., & Schaefer, H. F. 2000, *The Journal of Physical Chemistry A*, 104, 2273, doi: [10.1021/jp9918104](https://doi.org/10.1021/jp9918104)
- Riplinger, C., Pinski, P., Becker, U., Valeev, E. F., & Neese, F. 2016, *The Journal of Chemical Physics*, 144, 024109, doi: [10.1063/1.4939030](https://doi.org/10.1063/1.4939030)
- Sakai, N., & Yamamoto, S. 2013, *Chemical Reviews*, 113, 8981, doi: [10.1021/cr4001308](https://doi.org/10.1021/cr4001308)
- Seperuelo Duarte, E., Domaracka, A., Boduch, P., et al. 2010, *Astronomy and Astrophysics*, 512, A71, doi: [10.1051/0004-6361/200912899](https://doi.org/10.1051/0004-6361/200912899)
- Sie, N.-E., Cho, Y.-T., Huang, C.-H., et al. 2022, *The Astrophysical Journal*, 938, 48, doi: [10.3847/1538-4357/ac922a](https://doi.org/10.3847/1538-4357/ac922a)
- Sie, N.-E., Tsuge, M., Nakai, Y., & Watanabe, N. 2024, *Chem. Phys. Lett.*, 848, 141384, doi: [10.1016/j.cplett.2024.141384](https://doi.org/10.1016/j.cplett.2024.141384)
- Strazzulla, G., Brucato, J. R., Palumbo, M. E., & Spinella, F. 2007, *Memorie della Società Astronomica Italiana*, 78, 681
- Taquet, V., Charnley, S. B., & Sipilä, O. 2014, *The Astrophysical Journal*, 791, 1, doi: [10.1088/0004-637X/791/1/1](https://doi.org/10.1088/0004-637X/791/1/1)
- Tielens, A.G.G.M and Hagen, W. 1982, *Astronomy and Astrophysics*, 114, 245
- Tjossem, P. J., & Cool, T. A. 1985, *Symposium (International) on Combustion*, 20, 1321, doi: [10.1016/S0082-0784\(85\)80623-8](https://doi.org/10.1016/S0082-0784(85)80623-8)
- Trottier, A., & Brooks, R. L. 2004, *Astrophys. J.*, 612, 1214, doi: [10.1086/422680](https://doi.org/10.1086/422680)
- Tsuge, M., Molpeceres, G., Aikawa, Y., & Watanabe, N. 2023, *Nature Astronomy*, 1351, doi: [10.1038/s41550-023-02071-0](https://doi.org/10.1038/s41550-023-02071-0)
- Tsuge, M., Molpeceres, G., Aikawa, Y., & Watanabe, N. 2024, *Astrophys. J.*, 973, 80, doi: [10.3847/1538-4357/ad656a](https://doi.org/10.3847/1538-4357/ad656a)



- Tsuge, M., & Watanabe, N. 2023, Proceedings of the Japan Academy, Series B, 99, 103, doi: [10.2183/pjab.99.008](https://doi.org/10.2183/pjab.99.008)
- Varandas, A. J. C., & Rocha, C. M. R. 2018, Philosophical Transactions of the Royal Society A: Mathematical, Physical and Engineering Sciences, 376, 20170145, doi: [10.1098/rsta.2017.0145](https://doi.org/10.1098/rsta.2017.0145)
- Wang, J., Marks, J. H., Fortenberry, R. C., & Kaiser, R. I. 2024, Science Advances, 10, eadl3236, doi: [10.1126/sciadv.adl3236](https://doi.org/10.1126/sciadv.adl3236)
- Watanabe, N., Kimura, Y., Kouchi, A., et al. 2010, Astrophys. J. Lett., 714, L233, doi: [10.1088/2041-8205/714/2/L233](https://doi.org/10.1088/2041-8205/714/2/L233)
- Watanabe, N., & Kouchi, A. 2002, Astrophys. J., 571, L173, doi: [10.1086/341412](https://doi.org/10.1086/341412)
- Woon, D. E., & Dunning, T. H. 1994, The Journal of Chemical Physics, 100, 2975, doi: [10.1063/1.466439](https://doi.org/10.1063/1.466439)
- Yu, H. S., He, X., Li, S. L., & Truhlar, D. G. 2016, Chemical Science, 7, 5032, doi: [10.1039/c6sc00705h](https://doi.org/10.1039/c6sc00705h)
- Zhong, S., Barnes, E. C., & Petersson, G. A. 2008, The Journal of Chemical Physics, 129, 184116, doi: [10.1063/1.3009651](https://doi.org/10.1063/1.3009651)